Journal of Alloys and Compounds 509 (2011) 5426–5430

Contents lists available at ScienceDirect

Journal of Alloys and Compounds

journal homepage: www.elsevier.com/locate/jallcom

Sb doping behavior and its effect on crystal structure, conductivity and photoluminescence of ZnO film in depositing and annealing processes

T. Yang[a], B. Yao[a,b,*], T.T. Zhao[a], G.Z. Xing[a,c], H. Wang[a], H.L. Pan[a], R. Deng[a], Y.R. Sui[a], L.L. Gao[a], H.Z. Wang[a], T. Wu[c], D.Z. Shen[b]

[a] State Key Laboratory Superhard Material, and Department of Physics, Jilin University, Changchun 130023, PR China
[b] Key Laboratory of Excited State Processes, Changchun Institute of Optics, Fine Mechanics and Physics, Chinese Academy of Sciences, Changchun, 130033, PR China
[c] Division of Physics and Applied Physics, School of Physical and Mathematical Sciences, Nanyang Technological University 637371, Singapore

ARTICLE INFO

Article history:
Received 5 November 2010
Received in revised form 15 February 2011
Accepted 16 February 2011
Available online 23 February 2011

Keywords:
Sb-doping
p-type ZnO
Magnetron sputtering

ABSTRACT

The Sb-doped ZnO (ZnO:Sb) and undoped ZnO films with wurtzite structure and (0 0 2) preferred orientation were deposited on Si(1 0 0) substrate at 550 °C. It is deduced from XRD and XPS measurements that the Sb in the as-grown ZnO:Sb has high oxidation state and dopes in the form of oxygen-rich Sb–O clusters, which results in a large inner stress and a great increase of the *c*-axis lattice constant. After annealing at 750 °C under vacuum, the *c*-axis lattice constant of the ZnO:Sb decreases sharply to near the value of ZnO bulk, the electrical properties change from n-type to p-type and the PL intensity ratio of the visible to ultraviolet emission band goes down greatly, as the Sb content increases from 0 to 2.1 at.%. EDS and XRD measurements indicate that some of Sb dopants escape from the ZnO:Sb films and the oxygen-rich Sb-O clusters vanished after the annealing process. The effect of the change in Sb doping behavior on crystal structure, conductivity and PL is discussed in detail.

1. Introduction

ZnO is considered as a promising material for ultraviolet light-emitting diodes, laser diodes and photodetectors due to its many advanced physical properties, such as a wide band gap of 3.37 eV and a large exciton binding energy of 60 meV at room temperature, etc. [1–3]. Undoped ZnO is usually n-type conductive, which is associated with the presence of native point defects (e.g., oxygen vacancies (V_O) and interstitial zinc (Zn_i)) [4] or hydrogen impurities [5], but the fabrication of stable and reproducible p-type ZnO has been difficult due to the self-compensation and low solubility of acceptor dopants. In recent years, several groups have reported the growth of p-type ZnO by doping group V elements N [6,7], P [8], As [9] and Sb [10]. Among the group V elements, nitrogen has been regarded as the most suitable dopant for p-type ZnO due to its similar atomic radius to that of oxygen. However, numerous experimental efforts have suggested that stable and reproducible p-type ZnO is difficult to be prepared by N-doping. Moreover, Lyons et al. even reported that N is actually a deep acceptor in ZnO with an ionization energy of 1.3 eV [11]. Therefore, the suitability of N-doping for p-type conductivity in ZnO should be examined carefully.

On the other hand, Limpijumnong et al. [12] proposed that the large-size-mismatched impurities of group-V (As and Sb) as acceptors in ZnO do not stem from a simple substitution on the group VI-site, but from complexes of the type $As(Sb)_{Zn}–2V_{Zn}$ with low enthalpies of formation. A direct evidence for antimony as a zinc-site impurity in ZnO has been presented by Wahl et al. using the emission channeling technique [13]. A few groups have fabricated Sb-doped ZnO (ZnO:Sb) films [14–20], and even ZnO-based homojunction light-emitting diode with ZnO:Sb as p-type region [21]. However, we note that there are some abnormal properties of the ZnO:Sb films, and they were seldom discussed. For example, in the photoluminescence (PL) spectrum of ZnO:Sb film, the visible emission band was almost quenching [22], which is an abnormal phenomenon compared to the ZnO:N film.

In this work, Sb-doped ZnO films were fabricated at 550 °C by magnetron co-sputtering of Zn and Sb targets, and the undoped ZnO film was also fabricated by only sputtering of the Zn target for comparison. After the depositions, all of the films were annealed at 750 °C in vacuum. The structural, electrical and photoluminescence properties of the as-grown and annealed films are investigated. Moreover, the Sb doping behavior and its effect on ZnO films are also discussed in detail.

2. Experiment procedures

Sb-doped ZnO films were grown on Si(1 0 0) substrates by RF magnetron sputtering of a Sb (99.99%) target and DC magnetron sputtering of a Zn (99.999%)

* Corresponding author at: Department of Physics, Jilin University, Changchun 130012, PR China. Tel.: +86 13159640416; fax: +86 431 86171688.
E-mail address: binyao@jlu.edu.cn (B. Yao).

0925-8388/$ – see front matter © 2011 Elsevier B.V. All rights reserved.
doi:10.1016/j.jallcom.2011.02.080

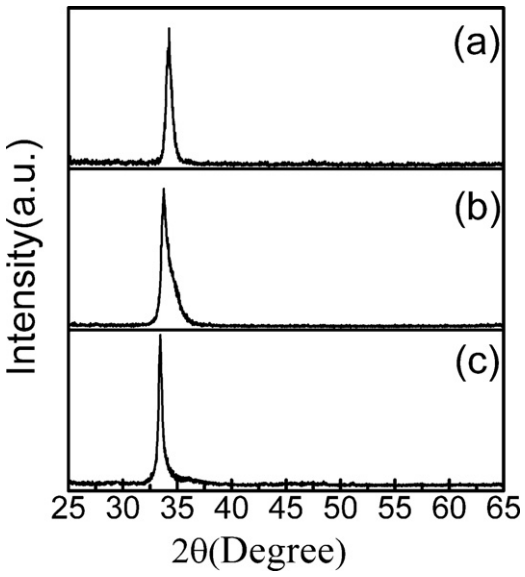

Fig. 1. XRD patterns of (a) sample A, (b) sample B and (c) sample C.

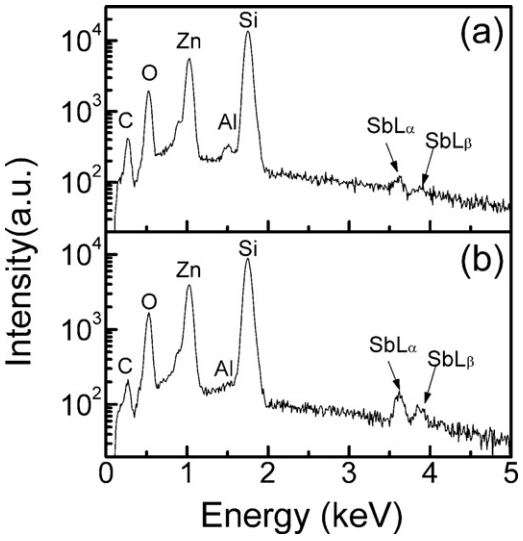

Fig. 2. EDS spectra of (a) sample B and (b) sample C. The signal of Si is attributed to substrate, and the signals of C, Al and Si are due to the electric conductive adhesive, sample stage used in our measurements.

target simultaneously. For comparison, the undoped ZnO film was also prepared on Si(1 0 0) substrate by DC magnetron sputtering of a Zn (99.999%) metal target. Before deposition, the substrates were treated with acetone, ethanol and deionized water in an ultrasonic bath, immersed in $H_3PO_4 + H_2SO_4$ (1:3) for 20 h and diluted HF solutions for 10 min in sequence, and finally blown dry with nitrogen (99.999%) gas. After that, the Si substrates were mounted in the growth chamber rapidly. The growth chamber was evacuated to a base pressure of 6×10^{-4} Pa, then Ar (99.999%) and O_2 (99.999%) with a molar ratio of 1:3 were introduced into the chamber as working gas, and the chamber pressure was fixed at 0.6 Pa during the whole deposition. The substrates were mounted on a rotating stage at 550 °C and kept a distance of 60 mm from the targets. Before the growth of each film, a layer of Zn was deposited on the substrate for 20 s to prohibit the oxidation of Si. Six samples were prepared in total. Sample A (undoped ZnO) is prepared by only sputtering of the Zn target. Samples B and C were prepared by co-sputtering of the Zn and Sb targets simultaneously, and the sputtering powers applied on Sb target were 25 W and 35 W for samples B and C, respectively. Slices of samples A, B and C were annealed at 750 °C in vacuum for 30 min, and they are labeled as sample D, E and F, respectively.

The structural and crystalline characterizations were performed by rotation anode X-ray diffractometer (XRD) (Rigaku D/Max-RA) with CuKα1 radiation ($\lambda = 0.15418$ nm), and the scan step size used is 0.02°. The composition of the ZnO:Sb films were analyzed by energy dispersive spectroscopy (EDS, GENESIS 2000 XMS 60S (EDAX Inc.)), and in our measurements the signals of C, Al and Si are due to the electric conductive adhesive (with carbon in it), sample stage (made by Al metal) and substrate. X-ray photoelectron spectroscopy (XPS) was performed by an ESCALAB 250 XPS instrument with Al Kα ($h\upsilon = 1486.6$ eV) X-ray radiation source, before measurements the films were etched by Ar^+ ions for 60 s, and all XPS spectra were calibrated by the C 1s peak (284.6 eV). The electrical properties were investigated by Hall measurement in the van der Pauw configuration at room temperature (Lakershore HMS 7707), and ohmic contacts of the electrodes were confirmed initially. The low temperature photoluminescence (PL) measurement was performed at 95 K by the UV Labran Infinity Spectrophotometer, which is excited by the 325 nm line of a He–Cd laser with a power of 50 mW.

3. Results and discussion

Fig. 1(a)–(c) shows the XRD patterns of samples A, B and C, respectively, which indicates that only one dominant diffraction peak is observed in each pattern, and the peak positions of samples A, B and C are 34.24°, 33.77° and 33.34°, respectively. The sample A is undoped ZnO (denoted as ZnO). Fig. 2(a) and (b) shows the EDS spectra of samples B and C, and the determined Sb contents of samples B and C are 3.2 and 5.1 at.%, respectively. Based on XRD results of Fig. 1 and discussion in the literatures reported previously, it is deduced that samples A, B and C have wurtzite structure with (0 0 2) preferred orientation. So the dominant peaks are (0 0 2) diffraction peaks. Using the diffraction data of the (0 0 2) peaks, the *c*-axis lattice constants of samples A, B and C are calculated to be 0.5238, 0.5308 and 0.5375 nm, respectively. The lattice constant of the sample A is slightly larger than that of ZnO bulk (0.5207 nm), which is usually ascribed to the in-plane compressive stress induced by the mismatch between the film and substrate [23]. However, the lattice constants of sample B and C are much larger than that of ZnO bulk and increase with the increase of Sb content, indicating that the great increment in the lattice constant is related to not only the mismatch, but also Sb content in the ZnO. Moreover, the effect of the Sb content on the lattice constant is dominant for the as-grown ZnO:Sb films.

In order to explain the great increment of the lattice constant of the ZnO:Sb, the chemical states of the elements in the sample C are identified by XPS. The binding energy of Zn $2p_{3/2}$ core level (XPS spectrum is not shown here) is 1021.8 eV, which is assigned to Zn-O bonds. Fig. 3 shows the XPS spectrum of Sb $3d_{3/2}$ core level of the sample C, which indicates a binding energy of 539.8 eV, corresponding to Sb^{5+} $3d_{3/2}$ [24], a high oxidation state of Sb atom in Sb-O bond. While the average bond length of Zn–O (L_{Zn-O}) is calculated to be 0.196 nm in the undoped ZnO (sample A) and the average bond length of Sb–O (L_{Sb-O}) is 0.200 nm [25]. If Sb atom occupies Zn site in the ZnO:Sb, the average bond length of the Zn–O (L_{dop})

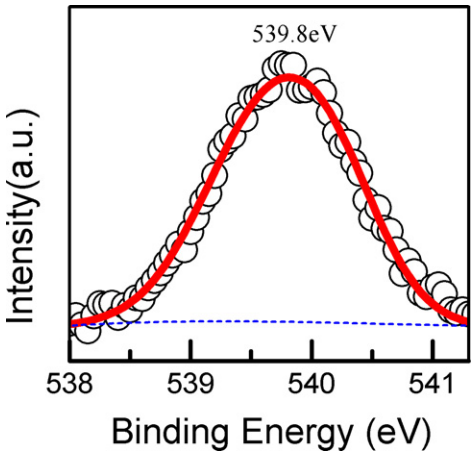

Fig. 3. XPS spectrum of Sb $3d_{3/2}$ core level of sample C. Black circles represent experimental data, red solid line corresponds with the Gauss fitting result, and the blue short dash line is the baseline. (For interpretation of the references to color in this figure legend, the reader is referred to the web version of the article.)

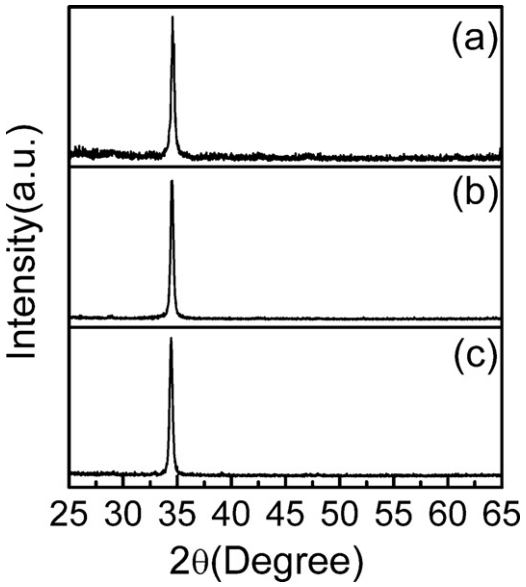

Fig. 4. XRD patterns of the (a) sample D, (b) sample E and (c) sample F.

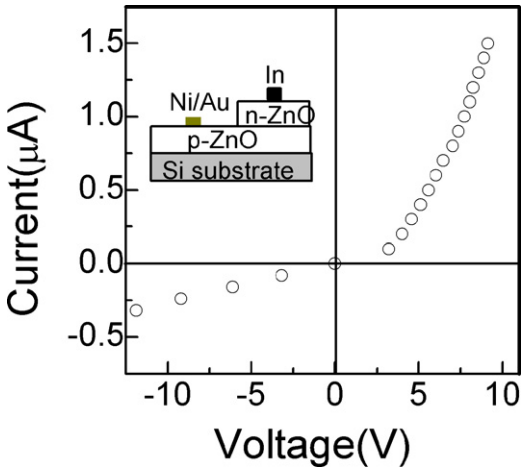

Fig. 5. *I–V* curve of the ZnO-based homojunction. The p-type region is the sample F, and n-type region is Al-doped ZnO film. The inset is the sketch of the homojunction.

should be in the range of 0.196–0.200 nm. By using the *c*-axis lattice constants calculated above, the L_{dop} of the samples B and C are estimated to be 0.199 nm and 0.201 nm, respectively. Since the average bond length of the ZnO for the sample C (0.201 nm) is larger than 0.200 nm, it is deduced that not all Sb dopants substitute for Zn in the sample C. For sample B, by using the average bond length of 0.196 nm and the Vegard's law:

$$L_{dop} = xL_{Sb-O} + (1-x)L_{Zn-O} \quad (1)$$

the Sb doping content x can be estimated to be 73.9 at.% when all Sb dopants occupy Zn sites. Obviously, the estimated Sb content is much larger than the measured value of 3.2 at.%, implying that the not all Sb dopants substitute Zn sites in the sample B, either. For the films were deposited in the oxygen-rich condition, the interstitial zinc (Zn_i) [26] can be excluded from the factors accounting for the larger lattice constants of ZnO:Sb films. Based on the above analysis, it is suggested that some Sb atoms in the ZnO:Sb may combine with oxygen atoms to form oxygen-rich Sb-O clusters [27], just like the nanoinclusions observed in Ag-doped ZnO [28], which induce large internal stress in the Sb-doped films, resulting in great increase in the lattice constant of the *c*-axis.

However, after the annealing at 750 °C under vacuum for 30 min, the diffraction peaks of the (0 0 2) peak shift towards high angle direction for all the annealed films (samples D, E and F) and the full width of half maximum (FWHM) decreases greatly, as shown in Fig. 4. By using the XRD data of Fig. 4, the *c*-axis lattice constants of all the annealed films are calculated to be close to that of ZnO bulk, implying that the *c*-axis lattice constants decrease after annealing. Hall measurement indicates that the as-grown films are high resistance, which is usually attributed to poor crystal quality. After the annealing, all the three samples change from high resistance to semi-conductivity. The electrical properties of samples D, E and F are listed in Table 1. It is found from Table 1 that both samples D and E show n-type conductivity, but the sample E (ZnO:Sb) has smaller carrier concentration and higher resistivity than sample D (undoped ZnO). While the sample F shows a p-type conductivity. In order to confirm the reliability of the p-type conductivity, a ZnO homojunction with Al doped ZnO as n-type region and the sample F as p-type region, as shown in the inset of Fig. 5, was fabricated. Fig. 5 indicates that the *I–V* curve of the homojunction shows a typical rectifying behavior, confirming the p-type conductivity of the sample F. The experiment results above indicate that the Sb-doping behavior changes during the annealing process and the change affects the properties of ZnO:Sb films.

In order to explore the mechanism of the change of Sb-doping behavior and its effects on structure, conductivity and photoluminescence properties of ZnO:Sb films, EDS, XPS and PL measurements were performed on the annealed ZnO:Sb films. The EDS spectra of samples E and F are shown in Fig. 6(a) and (b), respectively, and the Sb contents of the samples E and F are determined to be 1.0 and 2.1 at.%, which are much smaller than that of samples B and C, respectively, indicating that some of the Sb dopants evaporate during the annealing process. By using a multi-Gaussian fitting, the XPS spectrum of sample F (shown in Fig. 7) is resolved into two individual peaks at 539.0 and 539.8 eV, which correspond to Sb^{3+} $3d_{3/2}$ and Sb^{5+} $3d_{3/2}$ in Sb–O bonds [24], respectively. Because the *c*-axis lattice constants of samples E and F are close to that of the undoped sample D and the contents of 1.0 and 2.1 at.% are under the solubility limit of Sb in ZnO (3 at.%) [20], we believe that the Sb atoms in samples E and F should substitute Zn sites, implying the absence of oxygen-rich Sb–O clusters. The vanishing of the oxygen-rich Sb–O cluster releases the inner stress induced by Sb–O clusters, resulting in improvement of crystal quality of the annealed

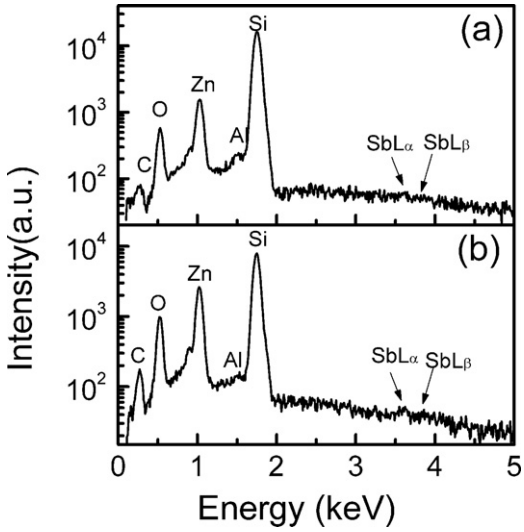

Fig. 6. EDS spectra of (a) sample E and (b) sample F. The signal of Si is attributed to substrate, and the signals of C, Al and Si are due to the electric conductive adhesive, sample stage used in our measurements.

Table 1
Electrical properties of the annealed films. The values 0, 1.0 and 2.1 at.% represent the Sb content in samples D, E and F, respectively.

Sb content (at.%)	Type	Resistivity (Ω cm)	Carrier density (cm^{-3})	Hall mobility ($cm^2 V^{-1} s^{-1}$)
0	n	4.63 E−1	2.47 E+18	5.53
1.0	n	1.86	9.54 E+17	3.56
2.1	p	2.82	1.12 E+18	2.02

ZnO:Sb, which is in agreement with FWHM decrease of ZnO:Sb after annealing.

As shown in Table 1, the annealed ZnO:Sb changes from n-type to p-type as the Sb content increases from 1.0 to 2.1 at.%. Many literatures in theory and experiment attribute p-type conductivity of the Sb-doped to the formation of acceptor complex composed by one substitution of Sb for Zn (Sb_{Zn}) and two Zn vacancies (V_{Zn}) (Sb_{Zn}–$2V_{Zn}$) due to its low formation energy and shallow acceptor level [12]. As predicted by Limpijumnong et al. [12], in the Sb_{Zn}–$2V_{Zn}$ complex Sb presents positive pentavalence (Sb^{5+}), which is also observed in our p-type conductivity film (sample F). Meanwhile, it is known that the oxygen-rich clusters are unstable at high temperature, so O atoms should be released during the annealing process [29], which is favorable to the formation of V_{Zn}. The higher the Sb content is, the more Sb_{Zn}–$2V_{Zn}$ complex acceptors can be formed and the more possible the formation of the p-type ZnO:Sb is. On the other hand, it is found from low-temperature PL spectra of the annealed samples shown in Fig. 8 that the PL intensity ratio of the visible to near-band-edge emission band decrease greatly as Sb incorporates into the ZnO and decrease gently with the increase of Sb content. Many research reports indicate that the visible emission band is related to native donor defects of the V_O and Zn_i [30] and the decrease in the intensity ratio implies decrease in amount of the V_O and Zn_i. Therefore, the results of Fig. 8 indicate that the amount of the V_O and Zn_i decrease with increasing the Sb content, leading to decrease of the compensation of the native donors for the Sb_{Zn}–$2V_{Zn}$ complex acceptor. As mentioned previously, when the oxygen-rich cluster is heated, O atom can be released, and consequently the decomposed O atoms could react with vacancy oxygen (V_O) and interstitial zinc (Zn_i), leading to the decrease in native defects of V_O and Zn_i. Therefore, the decomposition of oxygen-rich cluster is favorable to the decrease of native donor defects and formation of the Sb_{Zn}–$2V_{Zn}$ complex acceptor. It's noted in Fig. 7 that besides the main charge state of Sb: Sb^{5+}, there is Sb^{3+}. Based on the first-principle calculation results reported by

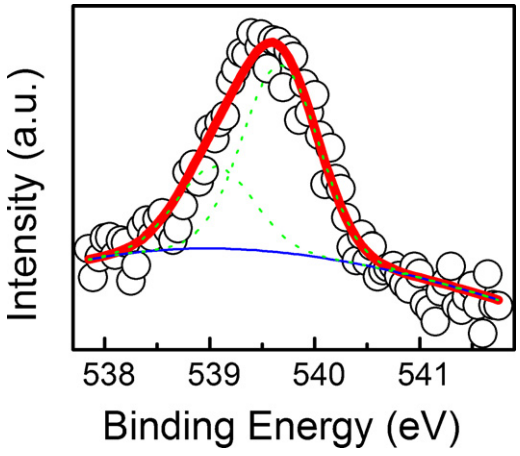

Fig. 7. XPS spectrum of Sb $3d_{3/2}$ core level of sample F. Black circles represent experimental data, red solid line corresponds with the Gauss fitting result, green dot lines are the Gauss fitting peaks and the blue short dash line is the baseline. (For interpretation of the references to color in this figure legend, the reader is referred to the web version of the article.)

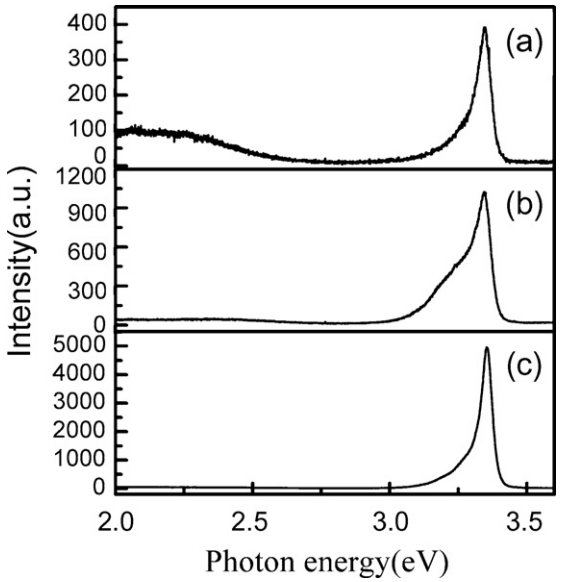

Fig. 8. The low-temperature (95 K) PL spectra of (a) sample D, (b) sample E and (c) sample F.

Limpijumnong et al., for the Sb^{3+} the following reaction should occur.

$$Sb_{Zn}^{+} + V_{Zn}^{2-} \rightarrow (Sb_{Zn}–V_{Zn})^{-} \quad (2)$$

Theoretically, the Sb_{Zn}–V_{Zn} (Sb^{3+}) complex could also be an acceptor, but the contribution of the $(Sb_{Zn}–2V_{Zn})^{-}$ may be larger than that of the $(Sb_{Zn}–V_{Zn})^{-}$ based on the XPS measurement results, because the Sb^{5+} is the main charge state of Sb dopants in the p-type conduction.

Based on above discussion, it is deduced that the formation of the p-type Sb-doped ZnO is due to the proper Sb doping content, decomposition of oxygen-rich Sb–O clusters by annealing and decrease in amount of the native donors of the V_O and Zn_i.

4. Conclusions

In summary, the structural, electrical and photoluminescence properties of the as-grown and annealed ZnO:Sb films are investigated. It is deduced from XRD and XPS measurements that the Sb in the as-grown ZnO:Sb has high oxidation state and dopes in the form of oxygen-rich Sb–O clusters, which results in large inner stress and a great increase of the *c*-axis lattice constant. After annealing at 750 °C, the *c*-axis lattice constant of the ZnO:Sb decreases sharply to near the value of ZnO bulk, the electrical properties change from n-type to p-type and the PL intensity ratio of the visible to ultraviolet emission band goes down greatly, as the Sb content increases from 0 to 2.1 at.%. EDS and XRD measurements indicate that some of Sb dopants escape from the ZnO:Sb films during annealing process, meanwhile, oxygen-rich Sb–O clusters should be decomposed and the Sb dopants in the annealed films should substitute at Zn sites. It is suggested that the change in Sb doping behavior induced by annealing decreases the inner stress and the amount of the native

donor defects (V_O and Zn_i) of the ZnO:Sb and improve formation possibility of Sb_{Zn}–$2V_{Zn}$ acceptor complex, which is responsible to the change in lattice constant, conductivity and PL of the annealed ZnO:Sb.

Acknowledgements

This work is supported by the Key Project of National Natural Science Foundation of China under grant no. 50532050, the "973" program under grant no. 2006CB604906, the Innovation Project of Chinese Academy of Sciences, the National Natural Science Foundation of China under grant nos. 6077601, 60506014, 10674133, 60806002 and 10874178, National Found for Fostering Talents of basic Science under grant no. J0730311.

References

[1] E.W. Wong, P.C. Searon, Appl. Phys. Lett. 74 (1999) 2939.
[2] P. Yu, Z.K. Tang, G.K.L. Wong, M. Kawasaki, A. Ohtomo, H. Koinuma, Y. Segawa, J. Cryst. Growth 601 (1998) 184–185.
[3] D.M. Bagnall, Y.F. Chen, Z. Zhu, T. Yao, S. Koyama, M.Y. Shen, T. Goto, Appl. Phys. Lett. 70 (1997) 2230.
[4] S.B. Zhang, S.H. Wei, A. Zunger, Phys. Rev. B 63 (2001) 075205.
[5] G. Chris, Van de Walle, Phys. Rev. Lett. 85 (2000) 1012.
[6] Y.R. Ryu, S. Zhu, D.C. Look, J.M. Wrobel, H.M. Jeong, H.W. White, J. Cryst. Growth 216 (2000) 330.
[7] J.F. Su, C.J. Tang, Q. Niu, C.Q. Wang, Z.X. Fu, J. Alloys Compd. 500 (2010) 5–8.
[8] K.K. Kim, H.S. Kim, D.K. Hwang, J.H. Hong, S.J. Park, Appl. Phys. Lett. 83 (2003) 63.
[9] Y.C. Huang, L.W. Weng, W.Y. Uen, S.M. Lan, Z.Y. Li, S.M. Liao, T.Y. Lin, T.N. Yang, J. Alloys Compd. 509 (2011) 1980–1983.
[10] Z. Yang, S. Chu, W.V. Chen, L. Li, J.Y. Kong, J.J. Ren, P.K.L. Yu, J.L. Liu, Appl. Phys. Express 3 (2010) 032101.
[11] J.L. Lyons, A. Janotti, C.G. Van de Valle, Appl. Phys. Lett. 95 (2009) 252105.
[12] S. Limpijumnong, S.B. Zhang, S.-H. Wei, C.H. Park, Phys. Rev. Lett. 92 (2004) 155504.
[13] U. Wahl, J.G. Correia, T. Mendonça, S. Decoster, Appl. Phys. Lett. 94 (2009) 261901.
[14] T. Aoki, Y. Shimizu, A. Miyake, A. Nakamura, Y. Nakanishi, Y. Hatanaka, Phys. Status Solidi (b) 229 (2002) 911–914.
[15] F.X. Xiu, Z. Yang, L.J. Mandalapu, D.T. Zhao, J.L. Liu, W.P. Beyermann, Appl. Phys. Lett. 87 (2005) 152101.
[16] E. Przeździecka, E. Kamińska, I. Pasternak, A. Piotrowska, J. Kossu, Phys. Rev. B 76 (2007) 193303.
[17] X.H. Pan, Z.Z. Ye, J.S. Li, X.Q. Gu, Y.J. Zeng, H.P. He, L.P. Zhu, Y. Che, Appl. Surf. Sci. 253 (2007) 5067–5069.
[18] W.W. Zhong, F.M. Liu, L.G. Cai, C.C. Zhou, P. Ding, H. Zhang, J. Alloys Compd. 499 (2010) 265–268.
[19] P. Wang, N.F. Chen, Z.G. Yin, F. Yang, C.T. Peng, J. Cryst. Growth 290 (2006) 56–60.
[20] D.H. Kim, N.G. Cho, K.S. Kim, S. Han, H.G. Kim, J. Electroceram. 22 (2009) 82–86.
[21] J.Z. Zhao, H.W. Liang, J.C. Sun, J.M. Bian, Q.J. Feng, L.Z. Hu, H.Q. Zhang, X.P. Liang, Y.M. Luo, G.T. Du, J. Phys. D: Appl. Phys. 41 (2008) 195110.
[22] J.Z. Zhao, H.W. Liang, J.C. Sun, Q.J. Feng, J.M. Bian, Z.W. Zhao, H.Q. Zhang, L.Z. Hu, G.T. Du, Electrochem. Solid-State Lett. 11 (2008) H323–H326.
[23] F. Conchon, P.O. Renault, P. Goudeau, E. Le Bourhis, et al., Thin Solid Films 518 (2010) 5237–5241.
[24] W.E. Morgan, W.J. Stec, J.R. Van Wazer, Inorg. Chem. 12 (1973) 953.
[25] P.A. Akishin, V.P. Spiridonov, Zh. Strukt. Khim. 2 (1961) 542.
[26] G.Z. Xing, B. Yao, C.X. Cong, T. Yang, Y.P. Xie, B.H. Li, D.Z. Shen, J. Alloys Compd. 457 (2008) 36–41.
[27] B. Kaiser, T.M. Bernhardt, M. Kinne, T.M. Bernhardt, M. Kinne, K. Rademann, J. Chem. Phys. 110 (1999) 1437–1449.
[28] O. Volnianska, P. Boguslawski, J. Kaczkowski, P. Jakubas, A. Jezierski, E. Kaminska, Phys. Rev. B 80 (2009) 245212.
[29] The melting point of antimony pentoxide is 380 °C (decomposes), http://en.wikipedia.org/wiki/Antimony_pentoxide.
[30] Ü. Özgür, Ya.I. Alivov, C. Liu, A. Teke, M.A. Reshchikov, S. Doğan, V. Avrutin, S.J. Cho, H. Morkoçd, J. Appl. Phys. 98 (2005) 041301.